machines

MDPI

Article

An Exergoeconomic Evaluation of an Innovative Polygeneration System Using a Solar-Driven Rankine Cycle Integrated with the Al-Qayyara Gas Turbine Power Plant and the Absorption Refrigeration Cycle

Wadah Talal and **Abdulrazzak Akroot** *

Branch of Mechanical Engineering, Faculty of Engineering, Karabük University, 78050 Karabük, Turkey; eng.wadah26@gmail.com
* Correspondence: abdulrazzakakroot@karabuk.edu.tr

Abstract: This study aims to develop, evaluate, and improve a polygeneration system that combines solar and Brayton cycle technologies and focuses on the sequential integration of heat. In this configuration, the exhaust gases from the Al-Qayyarah gas turbine power plant and the parabolic trough collector (PTC) array generate steam through a high recovery steam generation process. An absorption refrigeration system also supplies the Brayton circuit with low-temperature air. This process is evaluated from a 3E perspective, which includes exergy, energy, and exergoeconomic analyses for two different configurations. These configurations are integrated solar combined cycle (ISCC) with and without absorption systems (ISCC and ISCC-ARC). In addition, a comprehensive analysis was carried out to assess the impact of critical factors on the output generated, the unit cost of the products, and the exergy and energy efficiency for each configuration. The results revealed that the power produced by the ISCC-ARC and ISCC systems is 580.6 MW and 547.4 MW, respectively. Accordingly, the total energy and exergy efficiencies for the ISCC-ARC are 51.15% and 49.4%, respectively, while for the ISCC system, they are 50.89% and 49.14%, respectively. According to the results, the total specific costs for the ISCC-ARC system increased from 69.09 $/MWh in June to 79.05 $/MWh in December. ISCC's total specific costs also fluctuate throughout the year, from 72.56 $/MWh in June to 78.73 $/MWh in December.

Keywords: system; parabolic trough collectors; exergoeconomic; properties; 3E analysis; absorption system

Citation: Talal, W.; Akroot, A. An Exergoeconomic Evaluation of an Innovative Polygeneration System Using a Solar-Driven Rankine Cycle Integrated with the Al-Qayyara Gas Turbine Power Plant and the Absorption Refrigeration Cycle. *Machines* **2024**, *12*, 133. https://doi.org/10.3390/machines12020133

Academic Editor: Davide Astolfi

Received: 3 January 2024
Revised: 27 January 2024
Accepted: 31 January 2024
Published: 14 February 2024

1. Introduction

The urgency and significance of incorporating multiple energy production units into the use of a shared primary energy input effectively have been heightened due to the escalating concerns around global warming and fossil fuel depletion. In thermal power plants, such as gas turbine plants, fossil fuels are the principal energy source for electricity generation. Additionally, the waste flue gases produced during this process can be effectively utilized to power various other thermal cycles, including the steam and organic Rankine cycles, desalination cycles, absorption refrigeration cycles, and heating units, as well as other cycles. The field of integrated multi-energy production is now gaining significant attention and is considered a developing topic of study [1–3].

Although the demand for electricity has increased recently, there has been a noticeable shift towards sustainability. This shift is driven by heightened environmental consciousness, concerns regarding global warming, the depletion of natural resources, and the quest for energy autonomy. According to the Ministry of Energy's annual report in Iraq, Iraq has experienced a rapid annual growth in energy demand, growth reaching 4.5%. As a developing nation, Iraq boasts significant economic potential and a range of investment opportunities [1,4]. New power plants have been installed at an annual rate of 8%, pushing to fill the gap.

A study on the Iraqi electricity sector reveals that nearly 25% of electricity is produced by thermal plants, at 40% efficiency with 60% as wasted heat. Gas turbines, contributing 47% of Iraq's electricity, face efficiency challenges due to high temperatures. Implementing inlet air cooling systems is a recognized method for substantial electricity savings. Vapor Absorption Cooling technology [5] offers potential energy-saving solutions, yet remains unimplemented in Iraq's power plants.

High ambient temperatures in the inlet air result in a 6–10% decline in output power for every 10 °C temperature rise, with specific heat consumption increasing [6,7]. Although the Iraqi Ministry of Electricity encourages researchers to study the possibilities of improving current power plants and using renewable energy, there has been little research in this field.

Saeed et al. [8] examined the potential options for the replacement of fossil fuels in Iraq, with a particular emphasis on renewable energy sources and nuclear plants, and evaluated their viability for practical implementation. They provided a comprehensive analysis of how the implementation of alternative energy sources may effectively mitigate the current electricity supply deficit and make a significant contribution towards the reduction of greenhouse gas emissions resulting from the use of fossil fuel-based generators.

Hassan et al. [9] presented the feasibility of building solar photovoltaic power plants with a 20 MW capacity to generate energy. Their evaluation included four major cities in Iraq.

Kazem and Chaichan [10] researched the electrical shortages and a number of issues in Iraq. According to the results of this study, solar, wind, and biomass energy were all underutilized at the time; however, they have the potential to contribute significantly to Iraq's renewable energy future.

Talal and Akroot [11] presented an exergoeconomic study that was conducted to justify implementing an integrated solar combined cycle, ISCC, system utilizing the concentrated solar tower technology at the Al-Qayyarah power plant in Iraq.

Faisal et al. [12] presented an energy and exergy analysis carried out on a General Electric (GE) gas turbine unit in the Shatt Al-Basra power plant located in Basra, Iraq. Their analysis showed that the maximum thermal and exergy efficiencies occurred in February. According to the data, the best month to maximize thermal and exergy efficiency is February.

Salah et al. [13] analyzed the energy and exergy of the Kirkuk gas power plant to study the losses incurred under real operating circumstances.

Ahmed et al. [14] conducted a study on the energy and exergy analysis of a 150 MW gas turbine plant. The study used a Dataflow sheet and Kirkuk unit for the examination, in which the energy and exergy were investigated to assess the losses occurring under natural operating settings.

The study conducted by Alaa et al. [15] centered on the exergoeconomic analysis of the Taji power plant located in Baghdad. The selection of this station was motivated by the objective of mitigating the release of environmentally harmful waste gases, given its proximity to a residential area. Additionally, it aimed to enhance the generation of electrical power, addressing the longstanding issue of energy scarcity in Iraq.

By installing an absorption air refrigeration system at the compressor inlet, the incoming air can be treated at below ambient temperature. This improves the operating efficiency of the system, especially during times of high ambient temperatures [16–18]. It was observed that changes in ambient temperature have a significant effect on the productivity of gas turbines [19]. Researchers have noted that for every additional degree of the surrounding temperature, the performance and power production of the gas turbine diminished by approximately 0.07%, resulting in a reduction of 1.47 MW in power generation. This temperature-dependent behavior underscores the need for precise thermal management systems in gas turbine facilities to optimize their performance and maintain consistent power output, especially in regions with fluctuating climatic conditions [20].

To maximize the effectiveness of the interconnected systems, the solar Rankine cycle is designed to operate in tandem with a gas turbine power plant and the absorption refrigeration cycle. To define the implementation of this approach, various significant research papers are described in the following paragraphs.

A performance study of an integrated gas-, steam-, and organic fluid-cycle thermal power plant (IPP) was conducted by Oko and Njoku [21]. An integrated power plant is designed to harness the waste heat generated by the exhaust of a pre-existing 650 MW combined-cycle power plant (CCPP) that utilizes gas and steam. This waste heat was used to drive an organic Rankine cycle (ORC) unit, thereby enhancing the overall efficiency of the power generation process. The findings indicate that the waste heat-fired ORC unit produces an additional 12.4 MW of electric power. The exergy and energy efficiency of the integrated power plant (IPP) showed a significant increase compared to the extant combined cycle power plant (CCPP), with improvements of 1.95% and 1.93%, respectively.

Shukla and Singh [22] proved that gas turbine capacity can be increased by using an absorption chiller powered by waste heat, which could result in an 8–13% increase in power output. Compared to the expensive alternative of constructing a new gas turbine unit, this economical method increases the turbine's capacity by 11%, which is advantageous for energy producers in arid and tropical areas.

Elberry et al. [16] integrated an exhaust gas waste-heat-powered combined cycle with a Lith Br & Water absorption intake air refrigeration system. With model results verified by actual plant performance, this integration increases the electricity output by 11% when cooling down the inlet air from 30 °C to 10 °C. This also produces 3.5 g of condensed fresh water for every kilogram of intake air at 60% humidity.

Karaali [23] studied ammonia–water power cycles that efficiently utilize solar and waste heat and low-temperature heat sources. By conducting an energetic evaluation of a shared power and refrigeration cycle, they emphasized the use of ammonia (NH_3) with water mixes for independent power and cooling. This increase in a turbine's inlet pressure decreases both its energy and exergy efficiencies and its exergy efficiency.

Settino et al. [24] examined a gas combined cycle power plant integrated with solar energy. According to their analysis of the effect of the intercooler on power efficiency and CO_2 releases, a single-stage intercooler design with a ratio of compression reaching 17.9 provides a solar energy efficiency of 33% and a net electrical efficiency of 69.5%. The actual operating conditions in various cities result in annual efficiency of s solar energy to electricity around 32% and significant natural gas emissions of 7.7% to 5.8%.

Roshanzadeh et al. [25] examined the procedural operations of the combined cycle of a power plant at elevated temperatures and found reduced energy production. To address this issue, the use of solar-powered intake air cooling systems was explored to maintain performance and efficiency effectively. The ideal combination of vacuum plate collectors and double-acting absorption units was deemed economically attractive, with a return money period of 2.96 annually.

The aim of this article is to combine the absorption refrigeration cycle and solar-driven Rankine cycle with the Al-Qayyarah gas turbine power plant. This combined sysem merges solar energy, gas engine power, and cutting-edge cooling technologies to make the most of energy efficiency, reduce damage to the environment, and ensure a steady supply of electricity. This system is intended to cool the compressor's intake air and is driven by exhaust flue gases from the Heat Recovery Steam Generator (HRSG). This new method not only uses green energy sources but also makes the best use of traditional power production. The result is a more reliable and eco-friendly power plant that can keep abreast of the growing demand for electricity in Iraq. The Al-Qayyarah gas turbine power plant was selected as a case study. The power plant consists of six units with a capacity of 125 megawatts. In the current study, all calculations are performed for three units only. By applying the proposed solution model, this research has attempted to provide performance estimates for the completed integrated plant, considering different operating situations and local climates.

2. System Description

Figure 1 presents the configuration of the Al-Qayyarah gas-fired power plant. It consists of six 125-megawatt gas turbines, but we only use three units in this simulation. A gas turbine works very simply: air is compressed and mixed with fuel before being ignited to produce a high-temperature, high-pressure gases. This gases then expands in a turbine and extracts energy from it to drive the compressor and generate helpful energy.

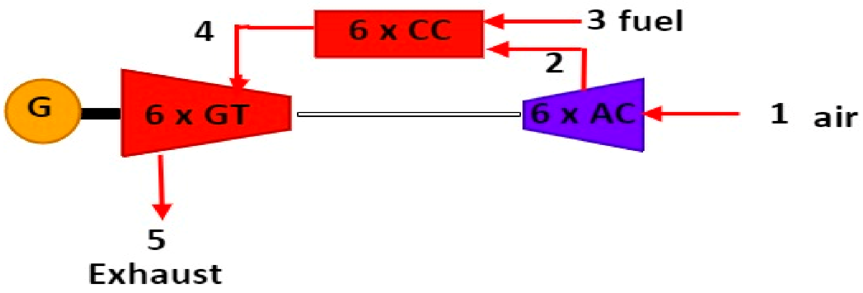

Figure 1. Al-Qayyarah gas power plant.

The exhaust gases from the gas turbine are routed through the steam generation process with heat recovery to generate additional electricity using the Rankine cycle and improve the system's overall efficiency. Figure 2 shows the integration of the combined cycle of Al-Qayyarah's gas turbines with parabolic trough collectors (PTCs) to increase the power plant's output by increasing steam generation in the HRSG. Only three units of gas turbine are used in this simulation.

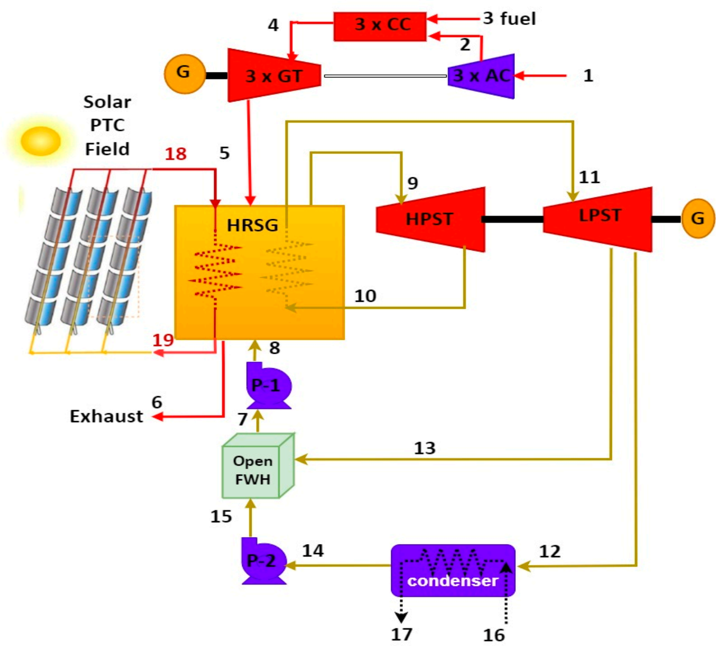

Figure 2. Al-Qayyarah integrated solar combined cycle.

Figure 3 presents the integrated solar combined cycle and the absorption refrigeration cycle (ISCC-ARC). The ARC cycle plays a central role as it uses the exhaust gases from the gas turbine in the HRSG unit as a heat source and lowers the temperature of the ambient air to 283 K before it enters the air compressors of the gas turbine units. The power generated by the ISCC-ARC system increases by reducing the power consumed by the air compressors, especially in summer.

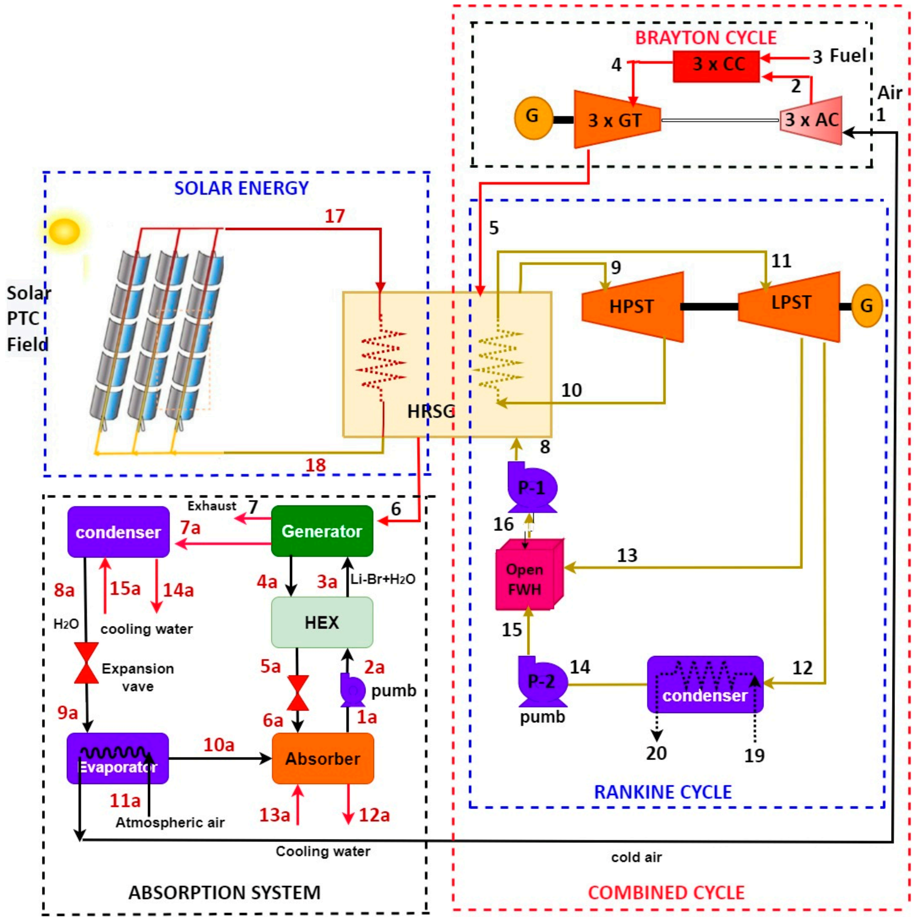

Figure 3. Integrated solar combined cycle with the absorption refrigeration cycle (ISCC-ARC).

3. Thermodynamics Model

This assessment uses the Engineering Equation Solver (EES) software version 10.2 for simulation and analysis. This program computes thermodynamic properties, such as pressure, temperature, entropy, and exergy. The assumptions made for this analysis are as follows:

- The system operates in a steady-state condition.
- Air is classified as an ideal gas.
- The pressure drop, heat loss, and friction effect of the pipe network and heat exchangers are all negligible.
- There are no changes in kinetic and potential energy, and the energies remain at zero.
- Compressors, turbines, and pumps are mathematically represented using adiabatic models that include a certain isentropic efficiency.

3.1. PTC System Model

The thermal power inlet to the accumulators' absorber is derived by [26]

$$\dot{Q}_{solar} = \eta_{PTC} \times A_{ap} \times DNI \tag{1}$$

The symbol η_{PTC} represents the efficiency of the PTC, with A_{ap} denoting the specific zone covered by the solar area. DNI refers to the direct normal irradiance recorded in Mosul (43.17° E, 35.33° N) during the relevant year. The primary function of the PTC involves the transmission of a fraction of the sunlight to the chief receiver in the form of solar isolation, and is denoted thus [27]:

$$\dot{Q}_{solar} = m_{Th\_VP} Cp_{Th\_VP} (T_{Th\_VP,out} - T_{Th\_VP,in}) \tag{2}$$

3.2. Thermodynamic Analysis

The mass and energy balance equations for each control volume (device) of the ISCC-ARC system may be expressed using the following relations [28]:

$$\sum \dot{m}_{in} = \sum \dot{m}_{out} \tag{3}$$

$$\dot{Q}_{in} + \sum \dot{m}_{in} h_{in} = \sum \dot{m}_{out} h_{out} + \dot{W}_{out} \tag{4}$$

where $\dot{Q}$, $\dot{W}$, h_{in}, and h_{out} are the rates of heat transfer, work, and specific enthalpy at the intake and the outlet per unit mass, respectively. The exergy destruction of each part is its magnitude, calculated using the equilibrium calculation of the exergy:

$$\dot{E}_q - \dot{E}_w = \sum \dot{E}_{out} - \sum \dot{E}_{in} - \dot{E}_D \tag{5}$$

where $\dot{E}_D$, $\dot{E}_q$, and $\dot{E}_w$ are, respectively, the exergy destruction rate, heat loss exergy rate, and the exergy of power. $\dot{E}_q$ and $\dot{E}_w$ are calculated thus:

$$\dot{E}_q = \left(1 - \frac{T_0}{T_i}\right)\dot{Q}_i \tag{6}$$

$$\dot{E}_w = \dot{W}_i \tag{7}$$

The energy and exergy stability relationships for all components of the ISCC-ARC system are shown in Table 1.

Table 1. Energy and exergy balance equations for all components of the ISCC-ARC system.

Component	**Energy Balances**	**Exergy Balances**
Compressor	$\dot{W}_{AC} = \dot{m}_{air}(h_2 - h_1)$	$\dot{E}_{D,AC} = \dot{W}_{AC} + \dot{E}_1 - \dot{E}_2$
Combustion chamber	$\dot{m}_{air}h_2 + \dot{m}_{fuel}LHV = (\dot{m}_{fuel} + \dot{m}_{air})h_4$	$\dot{E}_{D,CC} = \left(\dot{E}_2 + \dot{E}_3\right) - \dot{E}_4$
Gas turbine	$\dot{W}_{GT} = \dot{m}_4(h_4 - h_5)$	$\dot{E}_{D,GT} = \left(\dot{E}_4 - \dot{E}_5\right) - \dot{W}_{GT}$
HRSG	$Q_{HRSG} = \dot{m}_4(h_5 - h_6) + \dot{m}_{17}\left(\dot{h}_{17} - h_{18}\right)$	$\dot{E}_{D,HRSG} =$ $\dot{E}_5 - \dot{E}_6 + \dot{E}_8 - \dot{E}_9 + \dot{E}_{10} - \dot{E}_{11} + \dot{E}_{17} - \dot{E}_{18}$
HPST	$\dot{W}_{HPST} = \dot{m}_9(h_9 - h_{10})$	$\dot{E}_{D,HPST} = \dot{E}_9 - \dot{E}_{10} - \dot{W}_{HPST}$
LPST	$\dot{W}_{LPST} = \dot{m}_{11}(h_{11} - h_{13}) + \dot{m}_{12}(h_{13} - h_{12})$	$\dot{E}_{D,LPST} = \dot{E}_{11} - \dot{E}_{12} - \dot{E}_{13} - \dot{W}_{LPST}$
Condenser	$\dot{Q}_{Con} = \dot{m}_{14}(h_{12} - h_{14})$	$\dot{E}_{D,Con} = \dot{E}_{12} - \dot{E}_{14} + \dot{E}_{20} - \dot{E}_{19}$
Pump 1	$\dot{W}_{Pump1} = \dot{m}_7(h_8 - h_{16})$	$\dot{E}_{D,P1} = \dot{W}_{P1} + \dot{E}_{16} - \dot{E}_8$
Pump 2	$\dot{W}_{Pump2} = \dot{m}_{14}(h_{15} - h_{14})$	$\dot{E}_{D,P2} = \dot{W}_{P2} + \dot{E}_{14} - \dot{E}_{15}$
OFWH	$\dot{Q}_{OFWH} = \dot{m}_{15}(h_{16} - h_{15}) = \dot{m}_{13}(h_{13} - h_{16})$	$\dot{E}_{D,OFWH} = \dot{E}_{13} + \dot{E}_{15} - \dot{E}_{16}$
PTC	$\dot{Q}_{solar} = \eta_{PTC} \times A_{ap} \times DNI$	$\dot{E}_{Q,solar} = \left(1 - \frac{T_0}{T_{sun}}\right)\dot{Q}_{solar}$
Generator	$\dot{Q}_{Gen} = \dot{m}_{7a}h_{7a} + \dot{m}_{4a}h_{4a} - \dot{m}_{3a}h_{3a} = \dot{m}_6(h_6 - h_7)$	$\dot{E}_{D,Gen} = \dot{E}_6 - \dot{E}_7 + \dot{E}_{3a} - \dot{E}_{7a} - \dot{E}_{4a}$
Absorber	$\dot{Q}_{Abs} = \dot{m}_{10a}h_{10a} + \dot{m}_{6a}h_{6a} - \dot{m}_{1a}h_{1a}$	$\dot{E}_{D,Abs} = \dot{E}_{10a} - \dot{E}_{1a} + \dot{E}_{6a} + \dot{E}_{13a} - \dot{E}_{12a}$
HEX	$\dot{Q}_{HEX} = \dot{m}_{2a}(h_{3a} - h_{2a})$	$\dot{E}_{D,HEX} = \dot{E}_{4a} - \dot{E}_{5a} + \dot{E}_{2a} - \dot{E}_{3a}$

Table 1. *Cont.*

Component	Energy Balances	Exergy Balances
Pump 3	$\dot{W}_{P3} = \dot{m}_{1a}(h_{2a} - h_{1a})$	$\dot{E}_{D,P3} = \dot{W}_{P3} + \dot{E}_{2a} - \dot{E}_{1a}$
Evaporator	$\dot{Q}_{Evap} = \dot{m}_{10a}(h_{10a} - h_{9a})$	$\dot{E}_{D,Evap} = \dot{E}_{10a} - \dot{E}_{9a} - \dot{E}_{11a} + \dot{E}_{1}$
EV 1	$\dot{m}_{5a}h_{5a} = \dot{m}_{6a}h_{6a}$	$\dot{E}_{D,valv1} = \dot{E}_{5a} - \dot{E}_{6a}$
EV2	$\dot{m}_{8a}h_{8a} = \dot{m}_{9a}h_{9a}$	$\dot{E}_{D,valv2} = \dot{E}_{8a} - \dot{E}_{9a}$

Energy performance, η_I, can be estimated as follows [29]:

$$\eta_I = \frac{\dot{W}_{GT} - \dot{W}_{AC} + \dot{W}_{HPST} + \dot{W}_{LPST} - \dot{W}_{\dot{W}_{HPST}}}{\dot{Q}_{in}} \tag{8}$$

Exergy efficiency, η_{II}, is a measure of the system's quality and may be calculated using the following formula:

$$\eta_{II} = \frac{\dot{W}_{GT} - \dot{W}_{AC} + \dot{W}_{HPST} + \dot{W}_{LPST} - \dot{W}_{\dot{W}_{HPST}}}{E_{in}} \tag{9}$$

3.3. Investment Cost of the Main Equipment

Analysis of exergoeconomics involves establishing the price equilibrium for every component within the system. The essential equation used for the price equilibrium of every system section in thermoeconomics is depicted as follows [30]:

$$\sum_e \dot{C}_{e,k} + \dot{C}_{w,k} = +\sum_i \dot{C}_{i,k} + \dot{Z}_k \tag{10}$$

$$\dot{C}_j = c_j \dot{E}_j \tag{11}$$

where C is the cost rate ($/h) and $\dot{Z}_k$ is the entire cost rate related to capital investment and the operation and maintenance costs component k. The total investment cost rate is determined using the following formula:

$$\dot{Z}_k = \frac{Z_k \cdot CRF \cdot \varphi}{N \times 3600} \tag{12}$$

In this context, φ represents the maintenance factor, which is assigned a value of 1.06. N refers to the system's total number of operating hours in a year, namely 8000 h [31]. The Capital Recovery Factor (CRF) is a numerical value used to indicate the recovery of capital investment, and calculated thus:

$$CRF = \frac{(i(1+i)^n)}{((1+i)^n - 1)} \tag{13}$$

The interest rate, denoted as 'i' and the system life, denoted as 'n' are assumed to be 10% and 20 years, respectively [31]. The explicit equations for the cost balance of each component in this integrated system are listed in Table 2, together with their corresponding auxiliary equations and underlying assumptions. Furthermore, Table 3 lists the capital investment cost functions for each individual component in this system. The exergoeconomic analysis employs certain performance metrics to assess the system. The cost per unit exergy of fuel and product, the exergy destruction cost rate, and the exergoeconomic factor are defined as follows:

$$c_{F,k} = \dot{C}_{F,k} / \dot{E}_{F,k} \tag{14}$$

$$\mathrm{c_{P,k}} = \dot{\mathrm{C}}_{\mathrm{P,k}} / \dot{\mathrm{E}}_{\mathrm{P,k}} \tag{15}$$

$$\dot{\mathrm{C}}_{\mathrm{D,k}} = \mathrm{c_{F,k}} \dot{\mathrm{E}}_{\mathrm{D,k}} \tag{16}$$

$$\mathrm{r_k} = (\mathrm{c_{P,k}} - \mathrm{c_{F,k}}) / \mathrm{c_{F,k}} \tag{17}$$

$$\mathrm{f_k} = \dot{\mathrm{Z}}_{\mathrm{k}} / \left(\dot{\mathrm{Z}}_{\mathrm{k}} + \mathrm{c_{F,k}} \dot{\mathrm{E}}_{\mathrm{D,k}} + \dot{\mathrm{E}}_{\mathrm{L,k}} \right)) \tag{18}$$

Table 2. Cost analysis.

Component	**Exergetic Cost Rate Balance Equation**	**Auxiliary Equation**
AC	$\dot{C}_1 + \dot{C}_{W,AC} + \dot{Z}_{AC} = \dot{C}_2$	$c_{w,AC} = c_{w,GT}$
CC	$\dot{C}_2 + \dot{C}_3 + \dot{Z}_{CC} = \dot{C}_4$	$\frac{\dot{C}_2}{\dot{E}_2} = \frac{\dot{C}_4}{\dot{E}_4}$, $c_3 = 12$
GT	$\dot{C}_4 + \dot{Z}_{W,GT} = \dot{C}_5 + \dot{C}_{GT}$	$\frac{\dot{C}_4}{\dot{E}_4} = \frac{\dot{C}_5}{\dot{E}_5}$
HRSG	$\dot{C}_5 + \dot{C}_{17} + \dot{C}_8 + \dot{C}_{10} + \dot{Z}_{HRSG} =$ $\dot{C}_6 + \dot{C}_{18} + \dot{C}_9 + \dot{C}_{11}$	$\frac{\dot{C}_5}{\dot{E}_5} = \frac{\dot{C}_6}{\dot{E}_6}$
HPST	$\dot{C}_9 + \dot{Z}_{W,HPST} = \dot{C}_{10} + \dot{C}_{HPST}$	$\frac{\dot{C}_9}{\dot{E}_9} = \frac{\dot{C}_{10}}{\dot{E}_{10}}$
LPST	$\dot{C}_{11} + \dot{Z}_{W,LPST} = \dot{C}_{10} + \dot{C}_{11} + \dot{C}_{LPST}$	$\frac{\dot{C}_{11}}{\dot{E}_{11}} = \frac{\dot{C}_{12}}{\dot{E}_{12}} = \frac{\dot{C}_{13}}{\dot{E}_{13}}$
Condenser 1	$\dot{C}_{12} + \dot{C}_{19} + \dot{Z}_{cond1} = \dot{C}_{13} + \dot{C}_{20}$	$\frac{\dot{C}_{12}}{\dot{E}_{12}} = \frac{\dot{C}_{13}}{\dot{E}_{13}}$
Pump 1	$\dot{C}_{16} + \dot{C}_{W,P1} + \dot{Z}_{P1} = \dot{C}_8$	$c_{w,P1} = c_{w,HPST}$
Pump 2	$\dot{C}_{14} + \dot{C}_{W,P1} + \dot{Z}_{P1} = \dot{C}_{15}$	$c_{w,P2} = c_{w,HPST}$
OFWH	$\dot{C}_{13} + \dot{C}_{15} + \dot{Z}_{OFWH} = \dot{C}_{16}$	
PTC	$\dot{C}_{18} + \dot{C}_{q,solar} + \dot{Z}_{PTC} = \dot{C}_{17}$	$\dot{C}_{q,solar} = 0$
Generator	$\dot{C}_6 + \dot{C}_{3,a} + +\dot{Z}_{Gen} = \dot{C}_7 + \dot{C}_{7,a} + \dot{C}_{4,a}$	$\frac{\dot{C}_{4,a} - \dot{C}_{3,a}}{\dot{E}_{4,a} - \dot{E}_{3,a}} = \frac{\dot{C}_{7,a} - \dot{C}_{3,a}}{\dot{E}_{7,a} - \dot{E}_{3,a}}$
Pump 3	$\dot{C}_{1,a} + \dot{C}_{W,P3} + \dot{Z}_{P3} = \dot{C}_{2,a}$	$c_{w,P3} = c_{w,HPST}$
SHEX	$\dot{C}_{2,a} + \dot{C}_{4,a} + \dot{Z}_{SHEX} = \dot{C}_{3,a} + \dot{C}_{5,a}$	$\frac{\dot{C}_{4,a}}{\dot{E}_{4,a}} = \frac{\dot{C}_{5,a}}{\dot{E}_{5,a}}$
EV1	$\dot{C}_{5,a} + \dot{Z}_{EV1} = \dot{C}_{6,a}$	
Absorber	$\dot{C}_{6,a} + \dot{C}_{12,a} + \dot{Z}_{Abs} = \dot{C}_{1,a} + \dot{C}_{13,a}$	$\frac{\dot{C}_{6,a} + \dot{C}_{10,a}}{\dot{E}_{6,a} + \dot{E}_{10,a}} = \frac{\dot{C}_{1,a}}{\dot{E}_{1,a}}$, $c_{12,a} = 0$
Evaporator	$\dot{C}_{9,a} + \dot{C}_{11,a} + \dot{Z}_{Evap} = \dot{C}_1 + \dot{C}_{10,a}$	$\frac{\dot{C}_{7,a}}{\dot{E}_{7,a}} = \frac{\dot{C}_{8,a}}{\dot{E}_{8,a}}$, $c_{11,a} = 0$
EV2	$\dot{C}_{8,a} + \dot{Z}_{EV2} = \dot{C}_{9,a}$	
Condenser 2	$\dot{C}_{7,a} + \dot{C}_{14,a} + \dot{Z}_{cond2} = \dot{C}_{8,a} + \dot{C}_{15,a}$	$\frac{\dot{C}_{7,a}}{\dot{E}_{7,a}} = \frac{\dot{C}_{8,a}}{\dot{E}_{8,a}}$, $c_{15,a} = 0$

Table 3. Capital investment cost functions [27,32–34].

Part	Purchased Equation
AC	$(71.11 \times \dot{m}_{air} \times (Pr)) / \left(0.90 - \eta_{comp}\right) \times \ln(Pr)$
CC	$(25.6 \times \dot{m}_{air}) / (0.995 - P_4/P_2) \times [(1 + \exp(0.0181 \times T_4 - 26.41))]$
GT	$(266.3 \times \dot{m}_{gas}) / (0.921 - \eta_{turb}) \times \ln(Pr) \times [1 + \exp(0.0360 \times T_4 - 54.4)]$
HRSG	$6570\left[\left(\dot{Q}_{HRSG}/\Delta T_{LMTD}\right)^{0.8}\right] + 21276\dot{m}_{water} + 1184.4\dot{m}_g^{1.2}$
HPST	$6000\left(\dot{W}_{HPST}^{0.7}\right)$
LPST	$6000\left(\dot{W}_{LPST}^{0.7}\right)$
Pump 1	$3540\dot{W}_{P1}^{0.71}$
Pump 2	$3540\dot{W}_{P2}^{0.71}$
OFWH	$5200\dot{m}_{water}$
PTC	$126A_{hel}$
Generator	$17{,}500(A_G/100)^{0.6}$
Absorber	$16{,}000(A_{abs}/100)^{0.6}$
SHEX	$309.14(A_{SHEX})^{0.85}$
Pump 3	$17{,}585(W_{P3}/100)^{0.71}\left(1 + \frac{0.2}{1-\eta_{P3}}\right)$
Evaporator	$16{,}000(A_E/100)^{0.6}$
Ev1	$114.5\dot{m}_{water}$
Ev2	$114.5\dot{m}_{water}$

The total cost of the investment can be computed using the following equation [35]:

$$\dot{C}_{system} = \sum_{k=1}^{N} Z_k + \sum_{k=1}^{N} \dot{C}_{D,k} \quad (19)$$

The entire power price (electricity) over energy, \$/MJ, is calculated from the following formula [32]:

$$\dot{C}_{electricity,TOT} = \sum_{k=1}^{N} \dot{C}_{system}/\dot{W}_{net} \quad (20)$$

4. Results and Discussion

The exergoeconomic findings of the current integrated system are provided in three steps. In the first step, the integrated system functions according to selected circumstances, which serve as the base case. The second step involves conducting parametric experiments to analyze the behavior of this system under different scenarios, and the third step includes validating the integrated model by comparing this model with previous studies.

4.1. Base Case

The system is simulated in the Engineering Equation Solver (EES) program. Table 4 presents the primary parameters and simulation settings of the proposed ISCC-ARC system.

Table 4. Input values used for the ISCC-ARC system model [36–38].

	Factor	**Significance**
	Number of (GT) units	3
Brayton cycle	Ratio of compression	12.4
	Mass flowrate (kg/s)	(420 × 3)
	Gas inlet temperature (°C)	1090
	Atmosphere temperature (°C)	25
	Low-heat-value fuel (kJ.kg^{-1})	50,050
	η_{AC} (%)	85
	η_{GT}, (%)	87
	η_{CC}, (%)	99.51
Rankine cycle	High-pressure steam turbine (bar)	100
	Low-pressure steam turbine (bar)	20
	Condensate temperature (°C)	36
	η_{ST}, (%)	87
	η_{Pump}, (%)	82
	Effectiveness for HRSG (%)	72
ARS	Generator temperature (°C)	88
	Condenser temperature (°C)	39
	Absorber outlet temperature (°C)	48
	SHE effectiveness (%)	53
	Evaporator temperature (°C)	5
	Evaporator inlet air temperature (°C)	50
	Evaporator outlet air temperature (°C)	10
	Condenser inlet water temperature (°C)	25
	Condenser outlet water temperature (°C)	35
	Absorber inlet water temperature (°C)	25
	Absorber outlet water temperature (°C)	35
LiBr Solution	Solution strength (%)	53
Solar Area	Latitude (degrees)	35.36° N
	Longitude (degrees)	43.17° E
	Place	Mosul/Iraq
	Solar area (m^2)	510,130
	Outlet temperature (°C)	395
	Inlet temperature (°C)	295
	Heat transfer fluid	Therminol VP-1

The thermodynamic properties of the state points in the ISCC-ARC system model are presented in Table 5. This system model relies heavily on these characteristics when calculating exergy and energy. Also, the summary of the energy analysis is presented in Table 6.

Table 5. Properties for each state of the ISCC-ARC in ideal conditions.

State	Mass (kg/s)	Pressure (kPa)	Temperature (K)	Enthalpy (kJ/kg)	Entropy (KJ/kg. K)	Exergy (MW)
1	418	101.3	283	261.3	5.679	0
2	418	1277	632.7	621.8	5.774	138.8
3	7.573	101.3	288	−4672	11.53	392.6
4	425.6	1213	1360	235.4	8.036	406.8
5	425.6	104.5	822.9	−419.2	8.144	114.4
6	425.6	101.3	402.9	−885.1	7.365	15.04
7	665.4	371.5	101.3	−922.3	7.322	6.135
8	150.4	121.6	373.1	548.8	1.65	16.76
9	150.4	10,133	406.4	566.8	1.659	19.07
10	150.4	9829	794.9	3433	6.681	296.7
11	150.4	2007	581.8	3044	6.802	232.8
12	150.4	1946	774.9	3473	7.452	268.2
13	135.4	31	352.5	2645	7.81	114.8
14	15.04	121.6	463.4	2855	7.702	16.4
15	135.4	31	343	292.4	0.9533	8.504
16	135.4	121.6	343	292.6	0.9534	8.517
17	520.5	1000	665	780.6	1.675	146.5
18	520.5	1000	566	539.3	1.283	81.68
19	7038	101	283	41.39	0.1489	0
20	7038	101	295	91.66	0.3228	7.301
1a	85.21	310	0.8634	81.92	0.238	3.291
2a	85.21	310.2	6.944	81.93	0.238	3.291
3a	85.21	342.9	6.944	151.5	0.451	3.807
4a	72.84	361	6.944	219.6	0.4816	7.554
5a	72.84	333	6.944	167.2	0.3305	7.019
6a	72.84	321.6	0.8634	167.2	0.3306	7.017
7a	12.37	361	6.944	2656	7.506	3.291
8a	12.37	312	6.944	162.7	0.557	0.01654
9a	12.37	278	0.8634	162.7	0.586	−0.09024
10a	12.37	278	0.8634	2510	9.029	−2.179
11a	650	323	298	323.6	5.777	0.9202
12a	1845	298	308	104.3	0.3651	0.2987
13a	1845	308	298	146.1	0.5031	1.33
14a	2890	298	308	104.3	0.3651	0.4681
15a	2890	308	298	146.1	0.5031	2.084

Table 6. Output quantities produced by the integrated system model.

Output Quantity	ISCC	ISCC-ARC
Power supplied to ACs (MW)	486.98	451.984
Power output of GTs (MW)	836.63	835.832
Power output of HPST (MW)	56.144	56.136
Power output of LPST (MW)	143.544	143.516
Power supplied to P1 (kW)	1881	1881
Power supplied to P2 (kW)	18.96	18.96
Power supplied to P3 (kW)	-	0.08
Total work net of the system (MW)	547.4	581.6
Overall energy efficiency (%)	50.89	51.15
Overall exergy efficiency (%)	49.14	49.4

The primary exergy analysis findings for the various components of the performance and economics of the ISCC and ISCC-ARC are outlined in Table 7, offering comprehensive insights into the fuel, product, and destruction exergies associated with each specific element. Additionally, the table presents specific data on $\dot{E}_d$ and Ψ percentages, allowing for a detailed assessment of exergy performance. Notably, the net output power shows a standing corresponding to approximately 586.3 MW, followed by overall thermal efficiency ratios of 50.94%. Furthermore, the planned ISCC-ARC achieves a total η_{exergy} of 49.19%, with the electricity cost of the cycle being changed from 6876 $/h to 6708 $/h and the cost for each megawatt from 72.86 $/h to 71.16 $/h.

Table 7. Exergy analysis of the ISCC-ARC system model.

Part	$\dot{E}_F$ (MW)	$\dot{E}_P$ (MW)	$\dot{E}_{destruction}$ (MW)	$\dot{E}_{destruction}$ (%)	Ψ (%)
AC	525	416.5	35.42	5.071	92.16
CC	1594	1220	373.8	53.51	76.55
GT	877.1	835.8	41.25	5.905	95.3
HRSG	363	305.2	57.83	8.278	84.07
HPST	61.35	56.14	5.209	0.7457	91.51
LPST	163.6	143.5	20.06	2.871	87.74
Cond 1	71.56	6.828	64.74	9.267	9.541
OFWH	22.34	12.08	10.27	1.47	54.05
Pump 1	1.881	1.581	0.3001	0.04296	84.04
Pump 2	0.01896	0.01529	0.003669	0.0005253	80.64
PTC	139.4	64.79	74.64	10.68	46.47
Generator	9.926	1.727	8.199	1.181	17.4
Condenser	0.8035	0.3105	0.493	0.07105	38.64
Absorber	1.449	0.4865	0.9625	0.13873	33.58
HEX	0.1311	0.1266	0.004481	0.00064587	96.58
Pump 3	0.00008	0.00008	0.00000029	0.000000041	100
Evaporator	0.5125	0.167	0.3456	0.0498134	32.58
Ev1	0.004058	0.02214	0.262	0.0377636	84.51
Ev2	1.722	1.722	0.0005273	0.000076	99.97

Exergoeconomic analysis is a useful approach for evaluating the efficiency of a thermal system. The results of the exergoeconomic analysis for the ISCC-ARC system are shown in Table 8. The data suggest that the combustion chamber and air compressor had the greatest $\dot{Z}_K + \dot{C}_D$ values, respectively. The evaluation of the exergoeconomic component reveals that 58.9% of the total cost can be attributed to investment expenses, whereas only 42.1% can be attributed to the cost of exergy destruction.

Table 8. Exergoeconomic results of the components of the ISCC-ARC system.

Component	**c_f ($/GJ)**	**c_p ($/GJ)**	**$\dot{C}_D$ ($/h)**	**$\dot{Z}_K$ ($/h)**	**$\dot{Z}_K$+$\dot{C}_D$ ($/h)**	**f (%)**
AC	21.41	22.5	210.7	1107.4	1318	84.01
CC	14.94	19.51	1551	5.04	1556.04	0.03263
GT	19.51	20.73	223.6	781.2	1005	77.76
HRSG	18.32	20.44	294.4	506.9	801.3	63.26
HPST	21.86	24.87	31.63	197.1	228.73	86.17
LPST	21.17	24.87	118	380.16	489.16	76.32
Cond 1	21.17	222	380.7	3.98	384.7	1.036
OFWH	21.18	41.83	60.41	116.892	177.3	65.92
Pump 1	24.87	31.63	2.073	11.64	13.71	84.88
Pump 2	24.87	38.92	0.02534	0.445	0.473	94.61
PTC	0	12.87	0	1000.44	1000.44	100
Generator	0.008237	0.04758	0.2431	5.152	5.395	95.49
Absorber	0.01908	0.05698	0.06612	0.9432	1.009	93.45
HEX	0.04582	0.0475	0.00074	0.1	0.10074	99.24
Pump 3	24.93	0.01575	0	0.009	0.009	100
Evaporator	2.178	153.7	2.71	1.2456	3.956	31.49
Ev1	276.6	50.76	0.00006	0.0054	0.00547	98.9
Ev2	0.04582	0.04583	0.000087	0.03	0.03	99.73
Total System			2875.56	4118.763	6944.323	58.9

4.2. Results of the Parametric Studies

In this subsection, the findings of the conducted parametric studies on these integrated systems will be discussed. Figure 4 shows the effect of the pressure ratio (Pr) on the overall work and price of each component of the cycle. As shown in Figure 4a, Pr has a destructive impact on the $\dot{W}_{net}$ of every component in the cycle. When the Pr is high, the work consumed by the compressors increases. $\dot{W}_{net}$ in the ISCC-ARC system drops from 619.8 MW to 537.4 MW after the Pr is raised from 6 to 18. The results show that the $\dot{W}_{net}$ of the ISCC drops from 607.5 MW to 511.5 MW. Moreover, the results show that the performance of the ISCC with an absorption refrigeration cycle is higher than that of the ISCC system, because the absorption refrigeration system decreases the power consumed by the air compressors.

As shown in Figure 4b, the specific cost for both systems reduced as the Pr rose, peaked, and then increased with the further increase in the Pr. The figure also shows that Pr = 12 is the optimal pressure ratio. The specific cost of the ISCC-ARC system was 71.1 $/MWh at Pr = 12 compared to 72.8 $/MWh for the ISCC system. As the pressure ratio grows, both the investment cost rate of the BC components and the power consumed by the compressors also increase simultaneously. This increases the cost rate after reaching a pressure ratio of Pr = 12.

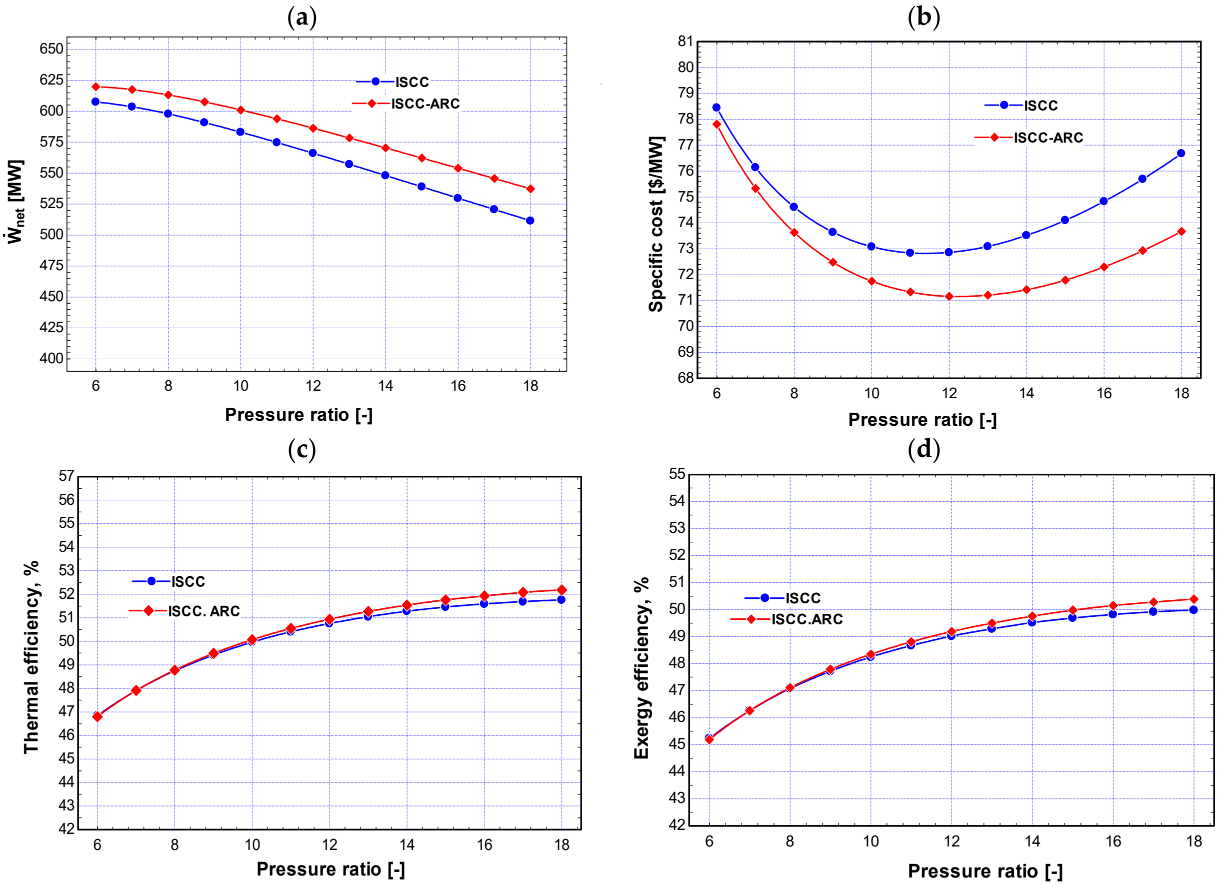

Figure 4. (**a**–**d**) Impact of the pressure ratio on the performance and cost of both systems.

It is evident from Figure 4c,d that Pr has an impact on the overall efficiencies of both systems. The diagrams illustrate how the overall efficiencies for both systems improve as the Pr rises. Depending on the results, when the Pr increases from 6 to 18, $\eta_{thermal}$ increases from 46.8% to 52.18%, and η_{exergy} increases from 45.19% to 50.39% for the ISCC-ARC system. Similarly, for the ISCC system, increases can be observed in $\eta_{thermal}$ from 46.84% to 51.76%, and in η_{exergy} from 45.23% to 49.98%.

Figure 5 shows the overall performance and costs of the ISCC-ARC and ISCC systems linked to the gas turbine inlet temperature (GTIT). These data demonstrate the influence of the GTIT on both the cost and performance of the gas cycle. The GTIT improves the effectiveness of the Rankine and Brayton cycles by raising the temperature of the exhaust gases and thermal energy at the gas turbine intake. Figure 5a shows the $\dot{W}_{net}$ increasing from 473.6 MW to 779.4 MW for the ISCC-ARC and from 452.7 MW to 758.6 MW for the ISCC system when the GTIT changes from 1250 K to 1550 K. The specific cost for both systems decreases when the GTIT rises, reaching a minimum value when the GTIT reaches 1517 K and increasing for a second time when the GTIT rises further (see Figure 5b). As the GTIT increases, the costs of the CC and GT likewise increase, leading to a corresponding rise in the specific costs of the systems. The specific cost of the ISCC-ARC system is 65.96 $/MWh at 1517 K of GTIT, while it is 67.17 $/MWh for the ISCC system.

The results shown in Figure 5c,d indicate that increasing the GTIT may enhance the thermal and exergy efficiencies of both systems. This is because a greater amount of energy input is effectively transformed into useful work, resulting in less energy being lost as low-quality heat.

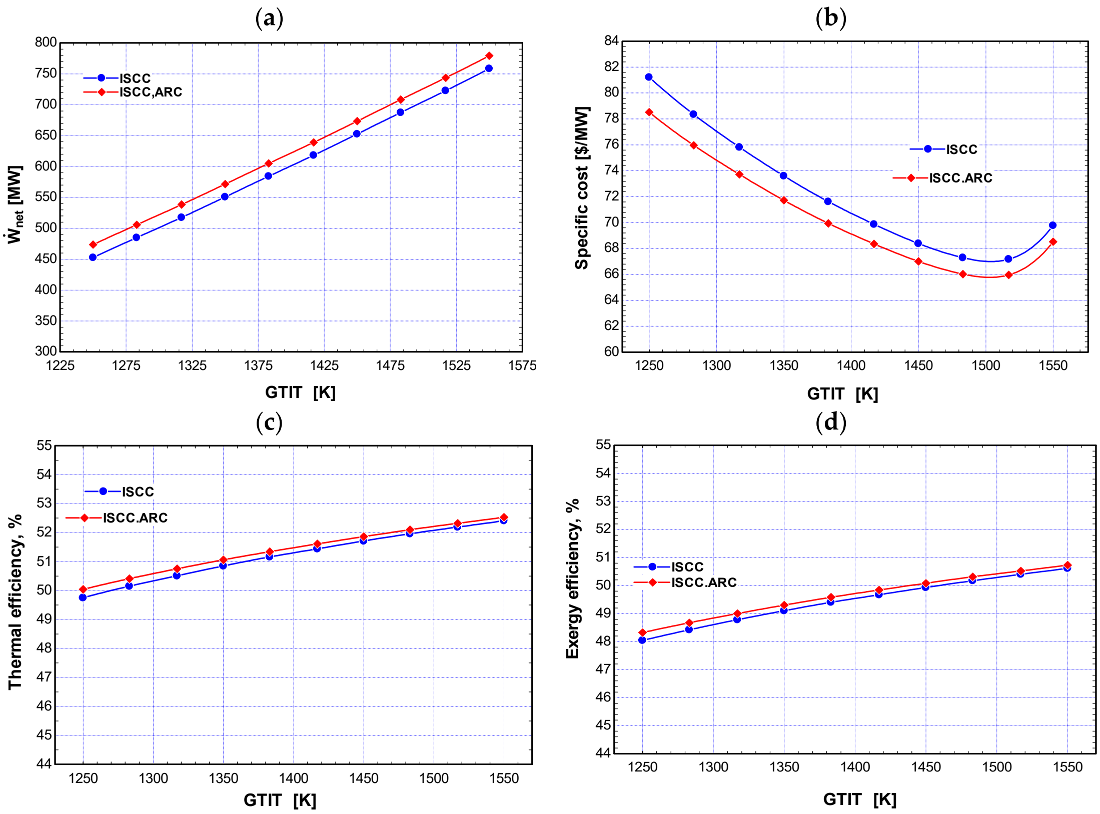

Figure 5. (**a**–**d**) Impact of GTIT on the performance and cost of both systems.

The effect of changing the pressure at the inlet of the HPST ($P_{HPST.in}$) on the work net, efficiencies, and cost of the ISCC-ARC and ISCC systems are shown in Figure 6. Increasing the $P_{HPST.in}$ increases the $\dot{W}_{net}$, $\eta_{thermal}$, and η_{exergy}, and reduces the specific costs of both systems. The performance of the systems is boosted at a higher $P_{HPST.in}$ due to the increase in the enthalpy. Figure 6a presents that, when $P_{HPST.in}$ rises from 80 bar to 125 bar, the $\dot{W}_{net}$ of the ISCC-ARC system rises from 578.2 MW to 584.4 MW. Likewise, the $\dot{W}_{net}$ of the ISCC system increases from 557.4 MW to 563.6 MW. As illustrated in Figure 6b, the specific cost for the ISCC-ARC system varies from 72.08 $/MWh to 70.43 $/MWh compared to the specific cost for the ISCC system changing from 73.94 $/MWh to 72.2 $/MWh. The overall efficiencies for both systems grow gradually when the $P_{HPST.in}$ rises, as seen in Figure 6c,d. When $P_{HPST.in}$ is raised from 80 bar to 125 bar, the $\eta_{thermal}$ in the ISCC-ARC system improves from 50.85% to 51.39%, and the η_{exergy} rises from 49.1% to 49.62%. In the ISCC system, the $\eta_{thermal}$ increases from 50.63% to 51.19%, while the η_{exergy} rises slightly from 48.89% to 49.43%.

Figure 7 illustrates the effect of changing the condenser temperature (T_{cond}) from 25 °C to 70 °C on the overall efficiencies, specific costs, and work net for both systems. The findings revealed that the increase in T_{cond} has a negative impact on the performance and specific cost of both systems. When the T_{cond} is high, the system's output is reduced, and the specific cost increases. Figure 7a shows that when the T_{cond} is raised from 25 °C to 70 °C, the $\dot{W}_{net}$ decreases from 587.4 MW to 561 MW for the ISCC-ARC system and drops from 566.6 MW to 540.2 MW for the ISCC system. The specific cost rose from 69.72 $/MWh to 77.04 $/MWh for the ISCC-ARC system, while it increased from 71.46 $/MWh to 79.15 $/MWh for the ISCC design, as presented in Figure 7b. Figure 7c,d illustrate a decline in the overall efficiencies of both designs due to a fall in the $\dot{W}_{net}$ as the T_{cond} increases. The results demonstrate that increasing the T_{cond} from 25 °C to 70 °C leads to a decrease in the $\eta_{thermal}$ from 51.66% to 49.33%, and a decrease in the η_{exergy} from 49.88% to 47.64% for the ISCC-ARC system. Furthermore, the $\eta_{thermal}$ in the ISCC system drops from 51.47% to 49.07%, while the η_{exergy} decreases from 49.7% to 47.38%.

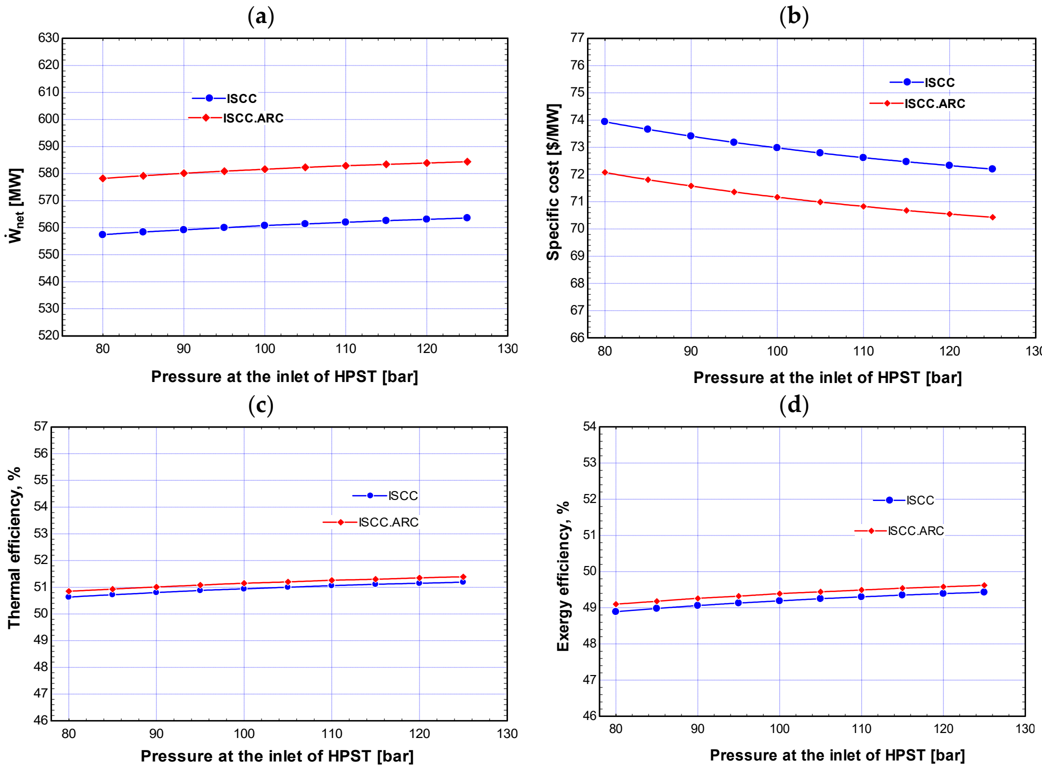

Figure 6. (**a**–**d**) Impact of $P_{HPST.in}$ on the performance and cost of both systems.

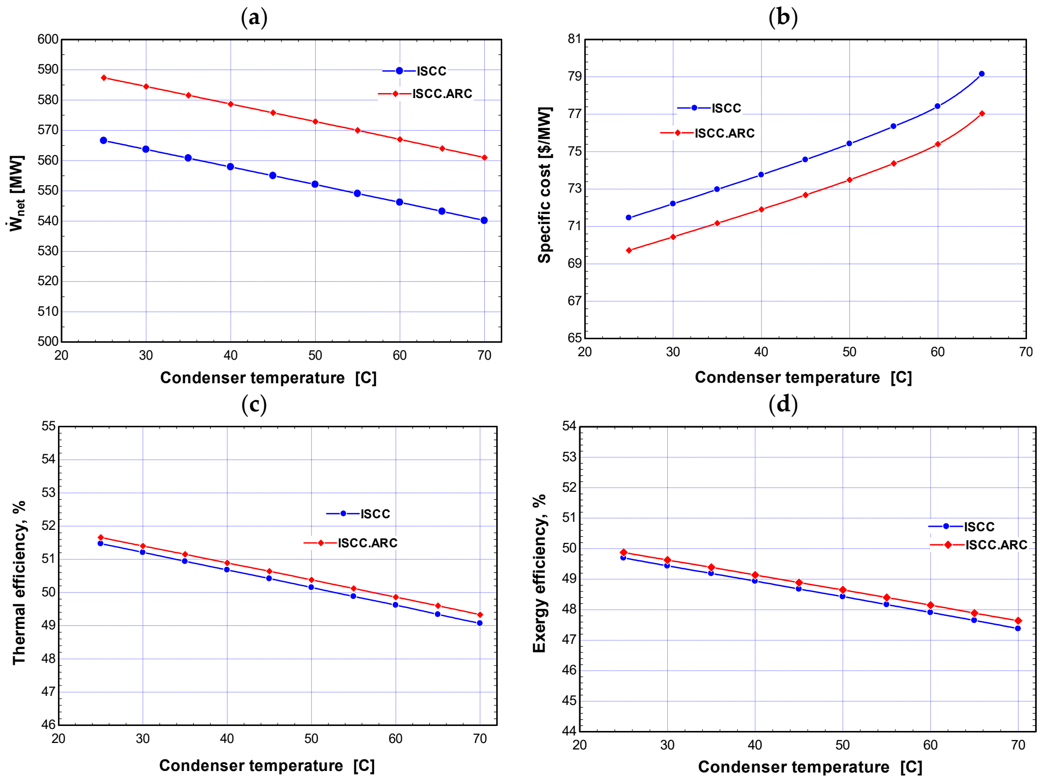

Figure 7. (**a**–**d**) Impact of T_{cond} on the performance and cost of both systems.

Figure 8 shows the proportion of monthly power production produced by both systems. The findings show that the power production of the ISCC system is better in the winter months due to the reduction in the atmospheric temperature and the gas turbine cycles, producing a maximum allowable work net. The ISCC system produced a maximum work net in March (557.7 MW). Conversely, the ISCC-ARC system exhibits enhanced power generation during the summer months due to the ability of the ARC system to lower the intake temperature of the air compressor and the high levels of direct normal irradiance (DNI). These settings optimize the outputs of the system throughout the summer months. In June, the ISCC system had its highest work net output of 591.4 MW.

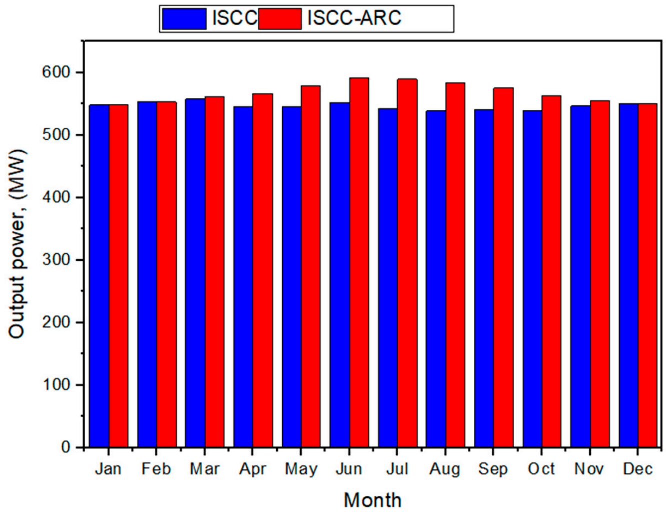

Figure 8. Total monthly output power from both systems.

Figure 9 illustrates the monthly specific costs of both systems. The visual representation makes it evident that changes in climate conditions exert a noticeable influence in terms of thermodynamic work on these cycles. Our study findings indicate that the overall specific costs for the ISCC-ARC system vary between 69.09 $/MWh in June and 79.05 $/MWh in December. Similarly, the overall specific costs for the ISCC vary from 72.56 $/MWh in June to 78.73 $/MWh in December.

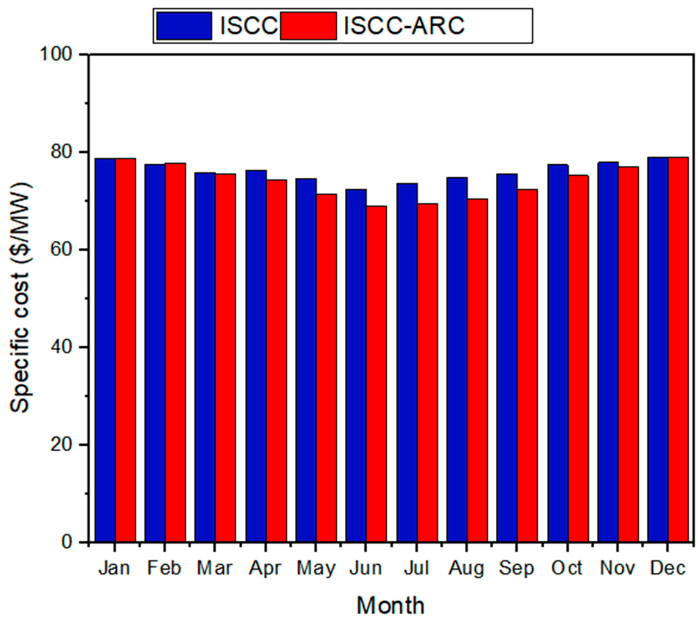

Figure 9. Monthly specific costs of both systems.

4.3. Validation Study Results

Table 9 presents a comparison between the production from Brayton model employed here in the study and the designated factors of the Brayton units within Al-Qayyarah station, illustrating the consistency. Correspondingly, as delineated in Table 9 the regenerative Rankine cycle (RC) model underwent a comparative analysis with the analogous cycle outlined in focusing on the validation of energy and efficiency [36].

Table 9. Validation results for the gas turbine's combined cycle.

Factor	Literature Model [37,38]	Current Model	Absolute Deviation (%)
$\dot{W}_{BC}$ (MW)	125 [37]	124.2	0.64
Exhaust temp (°C)	544 [37]	549	0.919
(%)	34.6 [37]	33.87	2.16
$\dot{W}_{RC}$ (kW)	55.780 [38]	55.239	0.97
η_{RC} (%)	30.14 [38]	29.16	1.8

The Schedule encompasses the operating environments utilized in the justification typical along with corresponding mathematical outcomes, affirming the robustness of the proposed model in contrast to the referenced findings.

5. Conclusions and Recommendations

This paper conducted a feasibility analysis of a new solar-assisted Brayton cycle (BC)-based Rankine cycle (RC) with an absorption refrigeration system (ARC). The integrated solar combined cycle with absorption refrigeration system was introduced and examined from the perspectives of exergoeconomics, exergy, and energy. The proposed model was composed of three gas turbine units, solar-based parabolic trough collectors, a Rankine cycle, and an absorption refrigeration system. The primary objective of the arranged system is to substantially augment the electricity generation capacity of the Qayyarah power plant, thereby addressing and mitigating the prevalent energy deficit in Iraq. The arranged system is also designed to optimize the operational efficiency of the Qayyarah station, implementing advanced technologies and methodologies to increase electricity output. The EES software was used to simulate and analyze the system. The essential findings are classified as follows:

- Adding the absorption refrigeration cycle improves the $\dot{W}_{net}$, $\eta_{thermal}$, and η_{exergy} of the ISCC-ARC system, the performance of which is far better than that of the ISCC system at keeping the temperature at the inlet of the air compressor at 10 °C, enhancing the $\dot{W}_{net}$, $\eta_{thermal}$, and η_{exergy} of the ISCC-ARC system. In contrast, the $\dot{W}_{net}$, $\eta_{thermal}$, and η_{exergy} of the ISCC system reduce with the increase in the ambient temperature. The work input to the compressor decreases from 315.2 MW to 271.5 MW due to maintaining the temperature of the intake air for the AC at 10 °C.
- The ISCC produces 547.4 MW, while the ISCC-ARC produces 581.6 MW. Adding an ARC to the system increases the produced output by 34.2 MW.
- The thermal and exergy efficiencies ($\eta_{thermal}$ and η_{exergy}) are, respectively, 50.89% and 49.14% for the ISCC system, whereas they increase to 51.15% and 46.4%, respectively, for the ISCC-ARC system.
- The highest exergy destruction of the elements in both systems is related to the combustion chambers because of their chemical reaction. The $\dot{E}_d$ for each element of the ISCC-ARC system is lower than that for the ISCC, except for the CC because the increase in the flow rate of fuel in the ISCC-ARC system causes an elevation in the $\dot{E}_d$ for the CC.
- A high steam turbine inlet pressure positively impacts cycle performance because the efficiencies and $\dot{W}_{net}$ of both systems increase as the $P_{HPST.in}$ increases.

- The gas turbine inlet temperature increases the thermal energy for the exhaust gases at the inlet of the GT, which leads to an increase in the $\dot{W}_{net}$ and efficiencies of both cycles.
- The overall specific costs for the ISCC-ARC system range from 69.09 $/MWh in June to 79.05 $/MWh in December. The overall specific costs of the ISCC also fluctuate during the year, from 72.56 $/MWh in June to 78.73 $/MWh in December.

Author Contributions: Conceptualization, W.T.; Methodology, W.T. and A.A.; Software, W.T. and A.A.; Validation, W.T.; Formal analysis, W.T. and A.A.; Resources, W.T.; Data curation, A.A.; Writing—original draft, W.T.; Writing—review & editing, A.A. All authors have read and agreed to the published version of the manuscript.

Funding: This research received no external funding.

Data Availability Statement: Data are contained within the article.

Conflicts of Interest: The authors declare no conflicts of interest.

Nomenclature

A_{ap}	Area of the solar field (m^2)
$\dot{C}$	Cost rate ($/h)
DNI	Direct normal irradiance of the sun
$\dot{E}$	Exergy rate (kJ)
$\dot{E}_D$	Exergy destruct
$\dot{E}_q$	Heat loss exergy
$\dot{E}_w$	Exergy of power
$\dot{m}$	Mass flow rate (kg/s)
h	Specific enthalpy ($kJ \cdot kg^{-1}$)
i	Interest rate
N	Number of operating hours
LHV	Lower heating value of fuel
$\dot{Q}$	Heat transfer rate (kW)
T	Temperature
Tcond	Condenser temperature
T_{sun}	DNI sun temperature
$\dot{W}$	Power (kW)
$\dot{Z}_k$	Entire cost rate
Greek Symbols	
η	Energy efficiency
η_I	Energy performance
η_{II}	Exergy efficiency
φ	Maintenance factor
Ψ	Exergy efficiency
Subscripts	
D	Destruction
e	Exit
i	Inlet
f	Fuel
p	Product
q	Related to heat
w	Related to work
tot	Total
Th_VP	Therminol VP-1

Abbreviations

AC	Air compressor
ARC	Absorption refrigeration cycle
BC	Brayton cycle
CC	Combustion chamber
CCPP	Combined cycle power plant
Con	Condenser
CRF	Capital Recovery Factor
CSP	Concentrating Solar Power
EES	Engineering Equation Solver
GE	General Electric
GT	Gas turbine
GTIT	Gas turbine inlet temperature
HRSG	Heat Recovery Steam Generation
HPST	High-pressure steam turbine
ISCC	Integrated solar combined cycle
ISCC-ARC	Integrated solar combined cycle with an absorption refrigeration cycle
LiBr	Lithium bromide
LPST	Low-pressure steam turbine
ORC	Organic Rankine cycle
Pr	Pressure ratio
PTC	Parabolic trough collector

References

1. Ibraheem, W.E.; Abdulraheem, A.A. Design of 5MW PV Power Plant in Iraq in Al-Sharqiyah Diyala Substation. In Proceedings of the 2021 Fourth International Conference on Electrical, Computer and Communication Technologies (ICECCT), Erode, India, 15–17 September 2021; pp. 1–7.
2. Dawood, T.A.; Raphael, R.; Barwari, I.; Akroot, A. Solar Energy and Factors Affecting the Efficiency and Performance of Panels in Erbil/Kurdistan. *Int. J. Heat Technol.* **2023**, *41*, 304–312. [CrossRef]
3. Khudhur, J.; Akroot, A.; Al-samari, A. Experimental Investigation of Direct Solar Photovoltaics that Drives Absorption Refrigeration System. *J. Adv. Res. Fluid Mech. Therm. Sci.* **2023**, *1*, 116–135. [CrossRef]
4. Abed, F.M.; Al-Douri, Y.; Al-Shahery, G.M. Review on the energy and renewable energy status in Iraq: The outlooks. *Renew. Sustain. Energy Rev.* **2014**, *39*, 816–827. [CrossRef]
5. Abusaibaa, G.Y.; Al-Aasam, A.B.; Al-Waeli, A.H.A.; Al-Fatlawi, A.W.A.; Sopian, K. Performance analysis of solar absorption cooling systems in Iraq. *Int. J. Renew. Energy Res.* **2020**, *10*, 223–230. [CrossRef]
6. U.S. Energy Information Administration (EIA). International Energy Outlook 2016. Available online: http://www.eia.gov/forecasts/ieo/ (accessed on 1 October 2023).
7. Haseeb, Q.S.; Yunus, S.M.; Shoshan, A.A.A.; Aziz, A.I. A study of the optimal form and orientation for more energy efficiency to mass model mult-istorey buildings of Kirkuk city, Iraq. *Alex. Eng. J.* **2023**, *71*, 731–741. [CrossRef]
8. Saeed, I.M.; Ramli, A.T.; Saleh, M.A. Assessment of sustainability in energy of Iraq, and achievable opportunities in the long run. *Renew. Sustain. Energy Rev.* **2016**, *58*, 1207–1215. [CrossRef]
9. Hassan, Q.; Hafedh, S.A.; Hasan, A.; Jaszczur, M. Evaluation of energy generation in Iraqi territory by solar photovoltaic power plants with a capacity of 20 MW. *Energy Harvest. Syst.* **2022**, *9*, 97–111. [CrossRef]
10. Kazem, H.A.; Chaichan, M.T. Status and future prospects of renewable energy in Iraq. *Renew. Sustain. Energy Rev.* **2012**, *16*, 6007–6012. [CrossRef]
11. Talal, W.; Akroot, A. Exergoeconomic Analysis of an Integrated Solar Combined Cycle in the Al-Qayara Power Plant in Iraq. *Processes* **2023**, *11*, 656. [CrossRef]
12. Faisal, S.H.; Naeem, N.K.; Jassim, A.A. Energy and exergy study of Shatt Al-Basra gas turbine power plant. *J. Phys. Conf. Ser.* **2021**, *1773*, 012020. [CrossRef]
13. Salah, S.A.; Abbas, E.F.; Ali, O.M.; Alwan, N.T.; Yaqoob, S.J.; Alayi, R. Evaluation of the gas turbine unit in the Kirkuk gas power plant to analyse the energy and exergy using ChemCad simulation. *Int. J. Low-Carbon Technol.* **2022**, *17*, 603–610. [CrossRef]
14. Ahmed, A.H.; Ahmed, A.M.; Hamid, Q.Y. Exergy and energy analysis of 150 MW gas turbine unit: A case study. *J. Adv. Res. Fluid Mech. Therm. Sci.* **2020**, *67*, 186–192.
15. Kareem, A.F.; Akroot, A.; Wahhab, H.A.A.; Talal, W.; Ghazal, R.M.; Alfaris, A. Exergo–Economic and Parametric Analysis of Waste Heat Recovery from Taji Gas Turbines Power Plant Using Rankine Cycle and Organic Rankine Cycle. *Sustainability* **2023**, *15*, 9376. [CrossRef]
16. Elberry, M.; Elsayed, A.; Teamah, M.; Abdel-Rahman, A.; Elsafty, A. Performance improvement of power plants using absorption cooling system. *Alex. Eng. J.* **2018**, *57*, 2679–2686. [CrossRef]

17. Santos, A.P.P.; Andrade, C.R.; Zaparoli, E. Comparison of different gas turbine inlet air cooling methods, World Academy of Science. *Eng. Technol.* **2012**, *6*, 1–6.
18. Kwon, H.M.; Kim, T.S.; Sohn, J.L.; Kang, D.W. Performance improvement of gas turbine combined cycle power plant by dual cooling of the inlet air and turbine coolant using an absorption chiller. *Energy* **2018**, *163*, 1050–1061. [CrossRef]
19. Javanfam, F.; Ghiasirad, H.; Khoshbakhti Saray, R. *Efficiency Improvement and Cost Analysis of a New Combined Absorption Cooling and Power System*; Springer International Publishing: New York, NY, USA, 2022. [CrossRef]
20. Sa, A.D.; Zubaidy, S.A. Gas turbine performance at varying ambient temperature. *Appl. Therm. Eng.* **2011**, *31*, 2735–2739. [CrossRef]
21. Oko, C.O.C.; Njoku, I. Performance analysis of an integrated gas-, steam- and organic fluid-cycle thermal power plant. *Energy* **2017**, *122*, 431–443. [CrossRef]
22. Shukla, A.K.; Singh, O. Effect of Compressor Inlet Temperature & Relative Humidity on Gas Turbine Cycle Performance. *Eng. Environ. Sci.* **2014**, *5*, 664–671.
23. Karaalı, R. Exergy analysis of a combined power and cooling cycle. *Acta Phys. Pol. A* **2016**, *130*, 209–213. [CrossRef]
24. Settino, J.; Ferraro, V.; Morrone, P. Energy analysis of novel hybrid solar and natural gas combined cycle plants. *Appl. Therm. Eng.* **2023**, *230*, 120673. [CrossRef]
25. Roshanzadeh, B.; Asadi, A.; Mohan, G. Technical and Economic Feasibility Analysis of Solar Inlet Air Cooling Systems for Combined Cycle Power Plants. *Energies* **2023**, *16*, 5352. [CrossRef]
26. Nami, H.; Mahmoudi, S.M.A.; Nemati, A. Exergy, economic and environmental impact assessment and optimization of a novel cogeneration system including a gas turbine, a supercritical CO2 and an organic Rankine cycle (GT-HRSG/SCO2). *Appl. Therm. Eng.* **2017**, *110*, 1315–1330. [CrossRef]
27. Bakhshmand, S.K.; Saray, R.K.; Bahlouli, K.; Eftekhari, H.; Ebrahimi, A. Exergoeconomic analysis and optimization of a triple-pressure combined cycle plant using evolutionary algorithm. *Energy* **2015**, *93*, 555–567. [CrossRef]
28. Akroot, A.; Namli, L. Performance assessment of an electrolyte-supported and anode-supported planar solid oxide fuel cells hybrid system. *J. Ther. Eng.* **2021**, *7*, 1921–1935. [CrossRef]
29. Nourpour, M.; Manesh, M.K. Evaluation of novel integrated combined cycle based on gas turbine-SOFC-geothermal-steam and organic Rankine cycles for gas turbo compressor station. *Energy Convers. Manag.* **2022**, *252*, 115050. [CrossRef]
30. Köse, A.; Koç, Y.; Yağlı, H. Energy, exergy, economy and environmental (4E) analysis and optimization of single, dual and triple configurations of the power systems: Rankine Cycle/Kalina Cycle, driven by a gas turbine. *Energy Convers. Manag.* **2021**, *227*, 113604. [CrossRef]
31. Mohammadkhani, F.; Shokati, N.; Mahmoudi, S.; Yari, M.; Rosen, M. Exergoeconomic assessment and parametric study of a Gas Turbine-Modular Helium Reactor combined with two Organic Rankine Cycles. *Energy* **2014**, *65*, 533–543. [CrossRef]
32. Cavalcanti, E.J.C. Exergoeconomic and exergoenvironmental analyses of an integrated solar combined cycle system. *Renew. Sustain. Energy Rev.* **2017**, *67*, 507–519. [CrossRef]
33. Li, Z.; Liu, L.; Jing, Y. Exergoeconomic analysis of solar absorption-subcooled compression hybrid cooling system. *Energy Convers. Manag.* **2017**, *144*, 205–216. [CrossRef]
34. Xie, N.; Xiao, Z.; Du, W.; Deng, C.; Liu, Z.; Yang, S. Thermodynamic and exergoeconomic analysis of a proton exchange membrane fuel cell/absorption chiller CCHP system based on biomass gasification. *Energy* **2023**, *262*, 125595. [CrossRef]
35. Musharavati, F.; Khanmohammadi, S.; Pakseresht, A. A novel multi-generation energy system based on geothermal energy source: Thermo-economic evaluation and optimization. *Energy Convers. Manag.* **2021**, *230*, 113829. [CrossRef]
36. Sachdeva, J.; Singh, O. Thermodynamic analysis of solar powered triple combined Brayton, Rankine and organic Rankine cycle for carbon free power. *Renew. Energy* **2019**, *139*, 765–780. [CrossRef]
37. Lugand, P.; Parietti, C. *Combined Cycle Plants with Frame 9F Gas Turbines*; American Society of Mechanical Engineers: New York, NY, USA, 1990; Volume 4, pp. 1–8. [CrossRef]
38. Moran, M.J.; Shapiro, H.N.; Boettner, D.D. *Fundamentals of Engineering Thermodynamics*; Wiley: Hoboken, NJ, USA, 2020. [CrossRef]